Low-energy magnetic excitations in Co/CoO core/shell nanoparticles

M. Feygenson, X. Teng, S. E. Inderhees, Y. Yiu, W. Du, W. Han, J. Wen, Z. Xu, A. A. Podlesnyak, J. L. Niedziela, M. Hagen, Y. Qiu, C. M. Brown, L. Zhang, and M. C. Aronson

Phys. Rev. B **83**, 174414 — Published 5 May 2011

DOI: 10.1103/PhysRevB.83.174414

Low Energy Magnetic Excitations in Co Core/CoO Shell Nanoparticles

M. Feygenson,[1] X. Teng,[2,3] S. E. Inderhees,[4] Y. Yiu,[1,5]W. Du,[3]W. Han,[2] J. Wen,[1] Z. Xu,[1]A. A. Podlesnyak,[6]J. L. Niedziela,[6] M. Hagen,[6] Y. Qiu,[7,8] C. M. Brown,[7] L. Zhang,[2]and M. C. Aronson[1,5*]

[1]*Condensed Matter Physics and Materials Science Department, Brookhaven National Laboratory, Upton, New York 11973, USA*

[2]*Center for Functional Nanomaterials, Brookhaven National Laboratory, Upton, New York 11973, USA*

[3]*Department of Chemical Engineering, University of New Hampshire, Durham, NH 03824, USA*

[4]*Department of Physics, University of Michigan, Ann Arbor MI 48109-1120, USA*

[5]*Department of Physics and Astronomy,Stony Brook University, Stony Brook NY 11794, USA*

[6]*Spallation Neutron Source, Oak Ridge National Laboratory, Oak Ridge, TN 37831, USA*

[7]*NIST Center for Neutron Research, National Institute of Standards and Technology, 100 Bureau Dr., Gaithersburg, MD 20899, USA and*

[8]*Department of Materials Science and Engineering, University of Maryland, College Park, MD 20742, USA*

(Dated: February 4, 2011)

We have used inelastic neutron scattering measurements to study the magnetic excitations of Co core/CoO shell nanoparticles for energies from 0-50 meV. Above the blocking temperature T_B, broad quasielastic scattering is observed, corresponding to the reorientation of the Co core moments and to paramagnetic CoO scattering. Below T_B, two nearly dispersionless inelastic peaks are found, whose energies increase with decreasing temperature as order parameters, controlled by the nanoparticle Néel temperature T_N=235 K, and saturating as T→0 at 2.7 meV and 6.7 meV, respectively. Similar excitations were observed in a powdered single crystal of CoO, indicating that both are intrinsic excitations of CoO, resulting from the exchange splitting of single ion states for T≤T_N. Pronounced finite size effects are observed for the scattering from the CoO nanoparticle shells, whose thicknesses range from 1.7-4.5 nm. These include an enhanced excitation linewidth, as well as a response that is not only spread over a much wider range of wave vectors, but is also significantly more intense in the nanoparticles than in bulk CoO.

PACS numbers: 75.75.Jn,78.79.Nx

I. INTRODUCTION

The utility of small ferromagnetic (FM) particles for magnetic recording applications requires that their moments must be stabilized against thermally induced reversal, most often by exchange coupling to an antiferromagnet (AF)[1–3]. We still have an incomplete understanding of this fundamental process. In equilibrium, is there a uniform reversal of the particle moment, or are there intermediate states where the magnetization is spatially modulated and transient[4–9]? How is the energy of reversal extracted from and returned to the thermal bath? What limits the rate at which the magnetization direction can be reversed? Finding answers to these questions will pave the way to designing improved nanoscaled devices where the moment is maximally stable in zero field, but can be switched as quickly as possible with the application of an external stimulus such as field, light, or current. Key to understanding the magnetic dynamics of nanoscaled systems is an experimental explication of their fundamental excitations, or normal modes, particularly on length scales that are smaller than the particle size and on time scales shorter than the moment reversal time[8,10,11]. These excitations are expected to be significantly altered from those of their bulk counterparts by finite size effects[12,13], impacting as well their equilibrium properties, such as the specific heat[12], the uniform magnetization[14], and the electrical and thermal conductivities.

Most experimental studies of the dynamics of magnetic particles have focussed on surface modes or modes with spatially uniform magnetization. At the highest temperatures, the nanoparticle magnetization changes direction via superparamagnetic fluctuations, evidenced by the broad and quasielastic scattering found in inelastic neutron scattering experiments[15–17]. Below a characteristic blocking temperature T_B, there is insufficient thermal energy in equilibrium to completely reverse the nanoparticle moment, which instead precesses in the presence of internal or external fields. The precession mode can be considered a q=0 spin wave, and its energies and lifetimes in different types of nanoscaled systems have been studied using inelastic neutron scattering[14,16,18–21], as well as Brillouin scattering[22–26] and ferromagnetic resonance experiments[25,27,28]. Precession modes have been studied in both ferromagnetic and antiferromagnetic nanoparticles, where the field in the latter case couples to the net moment of unterminated surface spins.

The challenges to observing magnetic excitations with nonzero wave vectors and energies pertinent to low temperature moment reversal are considerable. A basic limitation is that their wave length cannot exceed the particle size d, limiting experiments to wave vectors that are greater than π/d. The strong spin wave dispersions characteristic of ferromagnetic metals such as Co and Ni[29,30] consequently restrict these excitations to inconveniently

high energies for neutron scattering investigations when the particle size is ≈10 nm or less. More feasible are studies of antiferromagnetic particles, where the dispersion can be much weaker and a full range of nearly discrete excitations at different energies is possible.

We report here the results of inelastic neutron scattering experiments conducted on Co/CoO core-shell nanoparticles. At high temperatures, we detect the characteristic signatures of the reversal of the Co core magnetization, as well as paramagnetic scattering from the CoO shells. Below the blocking temperature, we observe a new magnetic mode that is inelastic and very weakly dispersing. We show that this excitation is also present in bulk CoO, although it has not previously been observed. CoO is an ideal benchmark system for comparing the excitations of nanoscaled and bulk systems, which have been extensively studied in the latter using triple axis neutron scattering[31–34] and optical spectroscopy[35–37] measurements, and where theoretical models for the underlying excitation structure are well developed[34,35,37–40] but still controversial.

Finite size effects can be expected to play a major role in the 1.7-4.5 nm thick CoO nanoparticle shells considered here. These effects are most familiar in the context of structure, where correlations with length scales larger than the shell dimension are absent from the bulk structure factor[41–43]. The range of correlations is further shortened by the nanoparticle form factor[44–46], and in many cases by the disordering of the nanoparticle surface, sometimes accompanied by the formation of long ranged defect structures[42]. When these considerations are extended to the magnetic structure, the net result is that magnetic Bragg peaks are substantially wider than their bulk analogs and the diffuse scattering background is enhanced[47]. The Scherrer formula is useful for approximating an average length scale from a diffraction peak for nanoparticles[48], but to obtain more detailed information about their structural modifications requires a more sophisticated treatment, such as the Pair Distribution Function approach[49].

Much less is known about the impact of finite size effects on the dynamics of nanoparticles. Most work has so far focussed on ferromagnetic particles[12,13,50], where the fundamental excitations are strongly dispersing in the bulk. In nanoscaled systems, the loss of translational invariance implies that the system eigenfunctions become a superposition of the bulk eigenfunctions with a wave vector distribution whose breadth increases with decreasing system size. While a separation of spin wave and particle-hole excitations is possible in bulk metallic ferromagnets, this is not the case in nanoscaled systems, leading to elementary spin excitations of considerable complexity. Also expected is a large scaled redistribution of spectral weight in nanoscaled systems to larger wave vectors and energies, relative to the bulk. At low energies, the anisotropy gap in the magnon spectrum generally increases with decreasing particle size, yielding a net increase in the average excitation energy[13,50]. At the same time, the dispersing nature of the magnetic excitations in metallic ferromagnets ensures that the high energy part of the magnetic response is spread over an increasing range of wave vectors and thus energies, shifting towards increasingly high energies as the system size decreases[12]. Finally, the lifetimes of the magnetic excitations are generally much shorter than their bulk counterparts. Variations in the profile of the magnetization within the particle, and especially at the particle surface itself, enhance the decay of magnetic excitations, in particular the q=0 precessing mode, producing pairs of excitations with nonzero wave vectors and energies.

There is currently very little theoretical and practical guidance for understanding how finite size effects affect the magnetic excitations of functional nanomagnetic particles, such as the exchange biased Co core/CoO shell nanoparticles that we study here. The length scales of these particles are sufficiently small that the magnetic excitations in these systems are expected to differ in significant ways from those of their bulk analogs[14,51], yet the length scales are sufficiently large that the direct calculation of magnetic eigenstates that is carried out in small systems like molecular magnets[52,53] becomes impossible. Further, understanding the underlying processes of core reversal and reorientation requires a knowledge of magnetic excitations with energies and wave vectors that correspond to spatial and temporal modulation of the core magnetization itself[8,10,11]. The experimental results that we report here provide the first insight into these magnetic modes in a flagship system for functional nanomagnetism, exchange biased Co core/CoO shell nanoparticles.

II. EXPERIMENTAL DETAILS

We synthesized bare Co nanoparticles in oleic acid[54,55] and oxidized them by bubbling oxygen for different times through the boiling solution at 180^o C. The resulting core-shell nanoparticles were precipitated by adding ethanol to the solution and the surfactant was subsequently removed by heating to 90^0 C in a vacuum oven. We also prepared a 24 g single crystal of CoO, using an image furnace under a partial oxygen pressure. This crystal was subsequently crushed to a fine powder for comparison to the nanoparticle samples. Magnetization measurements confirmed that the powder orders antiferromagnetically at the accepted Néel temperature of bulk CoO, T_N=293 K. No sign of contamination with Co_3O_4 was found in magnetization and powder x-ray measurements of the powdered bulk CoO crystal.

We have carried out an extensive characterization of the core-shell structure and its relationship to the magnetic properties of Co/CoO nanoparticles that were synthesized in the same way as those reported here. We combined electron microscopy, small-angle x-ray scattering and magnetization measurements to determine the core and shell dimensions of the nanoparticles, and as well to

TABLE I: Dimensions of the nanoparticle powders used in the neutron scattering measurements. R_{tot} and R_{core} are the radii of the nanoparticle and the Co core, respectively, and t_{shell} is the thickness of the CoO shell. H_{EB} is the 30 K exchange bias field.

sample	$R_{tot}(nm)$	$R_{core}(nm)$	$t_{shell}(nm)$	H_{EB}(Oe)
Co/CoO#1	3.6(0.4)	1.9(0.3)	1.7(0.3)	1500
Co/CoO#2	4.5(0.5)	2.5(0.4)	2.0(0.3)	6000
Co/CoO#3	5.5(0.5)	1.4(0.2)	4.1(0.5)	814
Co/CoO#4	5.5(0.5)	1.0(0.2)	4.5(0.5)	435
Co/CoO#5	4.2(0.5)	1.2(0.2)	3.0(0.5)	106

establish that particles grown using this low temperature synthesis and oxidation have core and shell dimensions that are highly monodispersed[47,55]. Direct examination using high resolution transmission electron microscopy show the near epitaxial quality of the core-shell interfaces, as well as their considerable directionality. Neutron diffraction measurements were previously carried out on a collection of similar Co core/CoO shell nanoparticle samples that included samples 1 and 2 of the current study, finding in each case that the Néel temperature $T_N \approx 235$ K[47]. The magnetic blocking temperature T_B separates the high temperature regime where the Co cores are superparamagnetic from the low temperature regime where core reversal is energetically blocked. T_B was experimentally defined as the temperature where the field cooled and zero field cooled magnetizations first separate, and where the exchange bias field H_{EB} first becomes nonzero. Despite their very different core and shell dimensions, T_B was determined to be ≈ 200 K in all five samples reported here, just as we found in our previous studies on similar Co/CoO core shell particles[55]. We believe that the lack of dependence of $T_B \approx (K(V)V)/k_B$ on the core volume V confirms the presence of a volume dependent magnetocrystalline anisotropy $K(V) \approx 1/V$, previously reported for Co particles smaller than 10 nm[56]. Dilution studies[55] found that T_B is independent of particle separation, indicating that the slowing of the core dynamics at T_B primarily results from the exchange interaction between the antiferromagnetic CoO shell and the ferromagnetic Co core, and not from interparticle interactions.

The properties of the five samples used in the neutron scattering measurements are summarized in Table 1. About 2 g of nanoparticle powders were loosely packed in aluminum foil and then placed in standard sample containers for the neutron scattering measurements. We performed zero field inelastic neutron scattering experiments on nanoparticle powders Co/CoO#1-4 at the NIST Center for Neutron Research, using the Disk Chopper Spectrometer (DCS) with an incident neutron wavelength λ_i=3.5 $\AA$. We used the Cold Neutron Chopper Spectrometer (CNCS) at the Spallation Neutron Source at Oak Ridge National Laboratory to perform similar measurements with λ_i=2.34 $\AA$ on Co/CoO#4/5, as well as on the powder of bulk CoO. In addition, we used the shorter wavelength of λ_i=1.22 $\AA$ at CNCS, in order to access excitations at energy transfers as large as 50 meV. The empty sample containers and a vanadium standard were measured using both DCS and CNCS at 300 K. The vanadium measurements were used to define the resolution functions of each instrument. The data were analyzed using the DAVE software[57], and were corrected for the dynamical factor k_i/k_F, the background, and the instrumental resolution. In some cases the data were symmetrized, transforming the scattered intensity to the imaginary part of the dynamical susceptibility $\chi''(q,E)$ by dividing through by the detailed balance factor.

III. EXPERIMENTAL RESULTS

An overview of the results is presented in Fig. 1a, which shows the energy E dependence of the scattered intensity I(E), integrated over wave vectors q, for temperatures above and below the blocking temperature T_B. At the highest temperatures, the scattering is broad and quasielastic. As the temperature is reduced, the quasielastic linewidth is reduced and the overall scattering intensity decreases. Interestingly, there is little dynamical signature of the onset of antiferromagnetic order at T_N. The scattering changes dramatically at T_B, where the quasielastic scattering collapses and is replaced by an inelastic peak that shifts to larger energies and becomes less intense as the temperature is reduced still further. For comparison, the dynamical susceptibility $\chi''(q,E)$ is presented for a range of temperatures above and below T_B in Fig. 1b, confirming that the inelastic excitation is present at the lowest temperatures. The reduction in its scattered intensity with decreasing temperature in I(q,E) is not the consequence of the detailed balance factor, but presumably reflects the transfer of spectral weight to the elastic line as the temperature is reduced further into the antiferromagnetic phase. To show that this result is representative for all measured wave vectors, the full energy and wave vector dependence of the scattered intensity I(q,E) is plotted for T=150 K in Fig. 1c. We see that the inelastic excitation is peaked near ± 3 meV, and shows very little dispersion, although its intensity increases strongly with increased wave vector q.

Different fitting functions are appropriate for describing the data above and below T_B, and we will treat these two temperature regimes separately. In all cases, however, the measured scattered intensity $I(\mathbf{q},E)$ of the Co/CoO nanoparticles was fitted by a theoretical scattering function $I_{theor.}(\mathbf{q},E)$,

$$I(\mathbf{q}, E) = C\,[I_{theor.}(\mathbf{q}, E) \otimes \Re(\mathbf{q}, E)] \qquad (1)$$

where C is the normalization constant, and $\Re(\mathbf{q},E)$ is the resolution function obtained from vanadium measurements. Different analytical expressions have been used to describe $I_{theor.}(\mathbf{q},E)$ above and below T_B.

We begin by describing the quasielastic scattering for T≥T_B. Fig. 2a shows that it consists of two separate components with very different widths: I_{Narrow}, which is only slightly broader than the experimental energy resolution, and I_{Broad}, which is responsible for the majority of the scattered intensity in this temperature range. I_{Broad} and I_{Narrow} are modeled by Lorentzian functions centered at 0 meV, giving

$$I_{theor.}(\mathbf{q},E) = \delta(\mathbf{q},0) + I_{Narrow}(\mathbf{q},E) + I_{Broad}(\mathbf{q},E) \quad (2)$$

The elastic scattering $\delta(\mathbf{q},0)$is given by a delta function, broadened by a resolution function that was obtained from measurements on a vanadium sample. An example of the fit quality is given in Fig. 2a. The narrow Lorentzian component is rather weak, but by comparing the fit in Fig. 2a, which includes the narrow Lorentzian, the broad Lorentzian, and the resolution broadened delta function of Eq. 2, to the fit represented in Fig. 2b, which includes all of these functions except the narrow Lorentzian, it is evident that both the broad and narrow Lorentzian components are required to produce the best fit to our data. We note that we fit only the neutron energy gain part of the DCS data, while the entire energy range was used in the CNCS data set.

The temperature dependence of the linewidth of the narrow Lorentzian, Γ_{Narrow} is plotted in Fig. 2c for two different samples. In both cases, Γ_{Narrow} decreases considerably between 325 K and 250 K, and this temperature dependence as well as its magnitude suggest, in accordance with previous reports[19,20,58–60], that I_{Narrow} represents scattering arising from superparamagnetic fluctuations of the Co core, where the core magnetization spontaneously reorients between two easy directions separated by an energy barrier $\epsilon(V_{Co}) = K(V_{Co})V_{Co}$. Here, V_{Co} is the Co core volume and K is the volume dependent anisotropy. These fluctuations become slower as the temperature is reduced, approaching the experimental energy resolution as T→T_B. The time scale $\tau \sim \hbar/\Gamma_{Narrow}$ of these superparamagnetic fluctuations is governed by an Arrhenius-like temperature dependence $\tau = \tau_0 exp(\epsilon/k_BT)$[61], giving $\epsilon(V_{Co})$ for the Co/CoO#3,4 samples of 62±6 and 61±3 meV, in good agreement with the value of 78 meV reported for bare Co nanoparticles of a similar size[56].

Fig. 2c shows that the behavior of the broad Lorentzian component I_{Broad} is very different, in that its linewidth Γ_{Broad} *increases* slightly with decreasing temperature. We ascribe this result to dynamical coupling between the Co core and CoO shell, and indeed it vanishes abruptly with the quasielastic scattering when the core dynamics freeze at T_B.

The emergence of the inelastic peak below T_B necessitates a different fitting function, as shown in Fig. 3a. Close inspection of the data indicates that there are two inelastic peaks present, one centered near ±3 meV and the second near ±6-7 meV. There is no evidence for residual quasielastic scattering on this temperature range, except possibly very close to T_B. Consequently, we used the following expression for T≤T_B:

$$I_{theor.}(\mathbf{q},E) = \delta(\mathbf{q},0) + I_{IN}(\mathbf{q},E\pm E_1) + I_{IN}(\mathbf{q},E\pm E_2) \quad (3)$$

where $\delta(\mathbf{q},0)$ is a delta-function describing the elastic scattering at E = 0 meV, while $I_{IN}(\mathbf{q},E\pm E_{1,2})$ is the sum of two Lorentzian functions describing inelastic excitations centered at E_1 and E_2, appearing for both neutron energy gain (E<0) and neutron energy loss (E>0):

$$I_{IN}(\mathbf{q},E\pm E_{i=1,2}) = \frac{\Gamma_1}{2\pi}\frac{A_1}{(E\pm E_1)^2+(\Gamma_1/2)^2} + \frac{\Gamma_2}{2\pi}\frac{A_2}{(E\pm E_2)^2+(\Gamma_2/2)^2} \quad (4)$$

The overall quality of the fits is demonstrated in Fig. 3a, where we have plotted the dynamical susceptibility χ''(q,E) at 50 K for a constant wave vector cut with a width of 0.12 $\AA^{-1}$ centered at q=1.27$\AA^{-1}$. We note that an alternative fit, where we have a single inelastic excitation at E_1 and a very broad quasielastic peak providing excess intensity above ∼6 meV provides a less accurate fit to the measured data, both at the lowest energies, and as well underestimates the scattering above ∼ 6 meV. The variation at 150 K of the two excitation energies E_1 and E_2 with wave vector is presented in Fig. 3b. The dispersions of the modes are very weak, approaching our experimental uncertainty. The temperature dependence of $\bar{E_1}$, obtained from fits of the scattered intensity I(q,E) integrated over all wave vectors, has the general appearance of an order parameter (Fig. 3c). $\bar{E_1}$ becomes nonzero below T≈T_N, and follows a mean-field temperature dependence, saturating at a constant value of 2.7±0.2 meV as T→0 K. The excitation at E_2 behaves similarly, approaching 6.7 meV as T→0. We observe no significant variation of the magnitude of $\bar{E_1}$ among the five different samples studied, and its resemblance to the antiferromagnetic order parameter previously determined by neutron diffraction measurements[47] indicates that this is an intrinsic excitation of the CoO shells, as we will discuss further below.

Previous neutron scattering measurements reported uniform precessional modes of both ferromagnetic and antiferromagnetic nanoparticles[59,62]. The energies of the inelastic modes reported here are too large to be explained as precessional modes, and their clear relationship to the CoO order parameter makes it imperative to carry out reference experiments on bulk CoO. The energy and wave vector dependencies of the scattered intensity I(q,E) for a powdered single crystal of CoO at 50 K is presented in Fig. 4a. Virtually all of the scattering is elastic, as might be expected for a bulk antiferromagnet for T≪T_N. Fig. 4a confirms that any quasielastic or inelastic scattering found in the energy range 0≤E≤10 meV is very weak. However, a more careful inspection (Fig. 4b) reveals the presence of inelastic scattering peaked near q=1.27 $\AA^{-1}$, corresponding to the magnitude of

q_{AF}=(2π/a)($\frac{1}{2}$,$\frac{1}{2}$,$\frac{1}{2}$), the primary antiferromagnetic wave vector of bulk CoO [63–66].

We have carefully analyzed the inelastic scattering intensity I(q,E) of powdered bulk CoO, and examples of our results for a wave vector cut centered at q_{AF} are shown in Fig. 5, both in the paramagnetic phase (300K, Fig. 5a) and in the antiferromagnetically ordered phase (50 K, Fig. 5b). For T≥T_N, the scattering is broad and quasielastic, implying that the similar scattering I_{Broad}(q,E) that we observed in the nanoparticles on this temperature range is also likely to be paramagnetic scattering from the CoO shells. We note that the 300 K data were obtained in air, so there is an unusually large background term for this data set. There are two distinct peaks near 3 meV and 5-6 meV evident in the 50 K data set, superposed on a broad and sloping background. Different fitting functions are required in the paramagnetic and antiferromagnetic phases. Below T_N=293 K, we used

$$I_{theor.}(\mathbf{q},E) = \delta(\mathbf{q},0) + I_{IN}(\mathbf{q},E+E_1) + I_{IN}(\mathbf{q},E+E_2) + I_{BKG}(\mathbf{q},E) \quad (5)$$

where $\delta(\mathbf{q},0)$ describes the elastic scattering, and $I_{IN}(\mathbf{q},E+E_1)$ and $I_{IN}(\mathbf{q},E+E_2)$ are two Lorentzian functions centered at E_1 ≈3 meV and at E_2 ≈5.7 meV, respectively. The third function $I_{BKG}(\mathbf{q},E)$ is a very broad Lorentzian centered at ≈ 4 meV, which we use to model the scattering background.

For the 300 K data we used a different function:

$$I_{theor.}(\mathbf{q},E) = \delta(\mathbf{q},0) + I_{Broad}(\mathbf{q},E) + I_{BKG}(\mathbf{q},E) \quad (6)$$

where $I_{Broad}(\mathbf{q},E)$ and $I_{BKG}(\mathbf{q},E)$ are two quasielastic Lorentzians centered at 0 meV.

The quality of these fits is demonstrated in Figs.5a and 5b. The energies of the inelastic excitations are similar to those found for the Co/CoO nanoparticles, but the excitations in powdered bulk CoO are only found for a limited range of wave vectors near q_{AF}. Fig. 6a compares I(q,E) and its fits at 50 K for three different wave vectors, 0.73$\AA^{-1}$, q_{AF}=1.27 $\AA^{-1}$, and 1.65 $\AA^{-1}$. Only the barest trace of the inelastic peak is present at 0.73$\AA^{-1}$, and it is wholly absent at 1.65 $\AA^{-1}$. The integrated intensity of the fitted inelastic peak, corrected for detailed balance, is strongest at the antiferromagnetic ordering wave vector q_{AF}=1.27 $\AA^{-1}$, and for temperatures above 50 K (Fig. 6b). We have compared E_1(q) and E_2(q) to the dispersions measured in the Co/CoO nanoparticles in Fig. 3b. E_1(q) is 15-20 % larger in bulk CoO than in the nanoparticles, and shows a similarly weak dispersion. Although our data span a somewhat limited range of temperatures, the temperature dependence of E_1, integrated over wave vectors 0.8≤q≤1.5 $\AA^{-1}$, is also consistent with a mean field expression, this one vanishing at the 293 K Néel temperature of bulk CoO, while saturating at 3.1 meV as T→0.

IV. DISCUSSION

While the excitation energies and their dispersions are very similar, there are some significant differences in the properties of CoO in the bulk and nanoparticle forms. We have plotted the wave vector integrated scattering intensity for both systems at 50 K in Fig. 7a, normalized by the mass of CoO. Two inelastic excitations are observed for both powdered bulk CoO and for the Co/CoO#4 nanoparticle sample, with E_1=3.1 meV and E_2=5.8 meV in powdered bulk CoO and E_1=2.7 meV and E_2=6.6 meV in the Co/CoO nanoparticles. Fig. 7a shows that both the E_1 and E_2 peaks are much broader in the nanoparticles than in the bulk powder. Fig. 3e compares the wave vector dependencies of the E_1 peak intensities, which are strongly peaked at the antiferromagnetic wave vector in bulk CoO, but increase monotonically with wave vector in all the nanoparticle systems. However, the most striking difference between the inelastic peaks in the two systems is the relative magnitudes of their intensities. Figs. 7a and 3e show that the E_1 peaks in the nanoparticle systems, normalized by the CoO mass, are as much as 500 times more intense than their analogs in powdered bulk CoO.

Before we begin our discussion of the physical origin of these excitations, we will establish an explicit comparison of intensities between our experiments and previous triple axis neutron scattering studies that were carried out on CoO crystals[31–34]. These latter experiments were either carried out at much higher energy transfers than ours, or found no excitations at the low energies of our experiments, focussing instead on the magnetic excitations found at energies of 20 -30 meV and above. To make the connection between the two sets of experiments explicit, we have carried out inelastic neutron scattering measurements on Co/CoO#4 and powdered bulk CoO at 150 K, using an incident neutron wave length of 1.22 $\AA$ to access energy transfers as large as 50 meV. The results were integrated over wave vectors and are compared for the two forms of CoO in Fig. 7 b,c. In both samples, two distinct peaks were observed at ≈ 20 meV and 30 meV, in reasonable agreement with previously reported spin wave energies[31–34]. Just as for the 3 meV E_1 peaks, we see that the linewidths of these higher energy magnetic excitations are substantially larger in the nanoparticle sample, although the excitation energies are only slightly shifted. Similarly, the integrated intensities of these peaks, when normalized by the CoO mass, are almost 40 times larger in the nanoparticle sample than in bulk CoO. These data make it clear why the 3 meV excitation has not been observed previously in the triple axis experiments on single crystals of CoO, as its intensity in powdered bulk CoO is ≈ 50 times weaker than that of the 20 meV peak. Indeed, the large counting rate of CNCS was absolutely indispensible for observing this excitation in powdered bulk CoO.

There has been considerable discussion of the magnetic excitations in CoO over the past 50 years, including

both theoretical analyses[38,39,67–70], and studies of the excitations by both inelastic neutron scattering and optical methods[31–37,71–74]. The basic model Hamiltonian for understanding the fundamental excitations in CoO was initially proposed by Kanamori[38], who observed that the orbital moment of Co^{2+} is not completely quenched by the crystal fields, so that the further action of the spin-orbit and exchange interactions ultimately determines the level spacing and dispersions that are observed in experiments. Sakurai[31] carried out the first inelastic neutron scattering experiments on a single crystal of CoO, finding two nearly q-independent bands of states between 27 and 31 meV, which he attributed to transitions among single ion levels split by exchange interactions in the antiferromagnetic state. In the following year, Daniel[35] performed infrared absorption measurements[35] that revealed additional structure within Sakurai's band of states, identifying excitations with q=0 energies at 26, 27, and 30 meV. Using a symmetry analysis and Kanamori's initial Hamiltonian, Daniel argued that the first neighbor exchange interaction J_1 is small, and that the second neighbor exchange J_2 was at least an order of magnitude smaller than that reported by Sakurai, consistent with the very weak dispersion observed in the neutron scattering measurements.

The relatively coarse energy resolution and limited access to low energies that were achieved by neutron scattering experiments in the 1960's precluded a more detailed analysis of the full spectrum of spin and orbital excitations that was presumed to be present. A recent series of inelastic neutron scattering experiments[32,34] has rekindled interest in the excitations of CoO by resolving a number of new magnetic excitations. The lack of excitations below 18 meV in this new generation of experiments leads to a somewhat different scenario than proposed by either Sakurai or Daniel, proposing that this 18 meV gap results from the mixing of the j=1/2 ground doublet and the j=3/2 spin orbit states by a large exchange J_2[34].

Our observation that the energies of the E_1 and E_2 excitations are proportional to the antiferromagnetic order parameter in both powdered bulk CoO and in Co/CoO nanoparticles suggests that these excitations are the direct consequence of the exchange splitting in the ordered state, comparable to the higher energy magnetic excitations studied most recently by Yamani[33,34]. The small magnitude of the excitation energy $E_1(q)$ and its almost complete lack of dispersion supports the previous conclusion that J_2 is small, and indeed a similarly small zone center excitation energy was predicted by Daniel[35]. We have considered the same expression for the excitation spectrum[35]:

$$E(\mathbf{q}) = \sqrt{E_0^2 + 2E_0V_1(\mathbf{q}) + 2E_0V_2(\mathbf{q})} \qquad (7)$$

$$\begin{aligned} V_1(\mathbf{q}) &= \textstyle\sum_{i'} V_{ii'} e^{i\mathbf{q}(\mathbf{r_i}-\mathbf{r_{i'}})} \\ V_2(\mathbf{q}) &= \textstyle\sum_{j} V_{ij} e^{i\mathbf{q}(\mathbf{r_i}-\mathbf{r_j})} \end{aligned} \qquad (8)$$

where $V_{ii'} = J_1\mathbf{S_i}\mathbf{S_j}$ is the exchange interaction between nearest neighbors and $V_{ij} = J_2\mathbf{S_i}\mathbf{S_j}$ is the exchange interaction between next-nearest neighbors. Obtaining a reasonable description of the dispersion $E_1(q)$ in powdered bulk CoO as well as in the Co/CoO nanoparticles (Fig. 3b), including its zone center value $E_0 \approx 3$ meV, requires values of the near neighbor exchange J_1=0.0087 meV, and the next nearest neighbor exchange J_2=0.013 meV that are even smaller than those that were previously proposed[35,72] on the basis of excitations with energies in the range 20-30 meV. We have highlighted in Table 2 the range of values that appear in the literature for the near neighbor and next neighbor exchange constants J_1 and J_2 in CoO, where our experimental results suggest a revision to values that are much smaller than those deduced from higher energy excitations. We note that these parameters and this model successfully produce two higher energy excitations at $\approx$ 21 meV and 32 meV, consistent with previous findings on this energy range[31,33,34].

TABLE II: Values of the nearest neighbor (J_1) and next nearest neighbor (J_2) exchange interactions deduced from fits to measured excitation energies and their dispersions.

J_1(meV)	J_2(meV)	Ref.
0.0062	0.013	Co/CoO np (this work)
0.0087	0.013	CoO bulk (this work)
0.0087	0.15	[35]
0.087	1.44	[31]
0.54	1.86	[38,68]
0.25	2.4	[75]
-0.31	2.8	[32]
0.29	0.66	[73]

Based on this comparison of bulk and nanoscaled CoO, we conclude that the E_1 and E_2 excitations have the same origins in both systems, namely that they result from the exchange splitting of single ion energy levels. The excitation energies differ by $\approx$ 15% in bulk and nanoscaled CoO, and their temperature dependencies follow the order parameters dictated by their respective Néel temperatures. In both cases, the excitations have similarly weak dispersions. It is perhaps surprising that these excitations have such similar properties in bulk CoO and in Co/CoO core-shell nanoparticles, where the CoO shells are less than 2 nm thick. The relative weakness of the exchange coupling relative to crystal field and spin orbit energies in CoO is responsible for the minimal dispersion of the spin waves, and we conjecture that this predominantly local character of these excitations makes them more resistant to finite size effects than the strongly dispersing magnetic excitations found in metallic magnets, where these effects can be very large [13,50].

While the basic excitations appear to have the same origins in bulk and nanoscaled CoO, there are clear signatures of finite size effects in the latter. Fig. 8 compares the linewidths Γ_1 of the E_1 inelastic peaks in bulk and nanoscaled CoO. Γ_1 increases gradually with wave vector in bulk and nanoscaled CoO, consistent with the conventional scenario for bulk antiferromagnets[76]. The

excitation linewidths are as much as a factor of four larger in the nanoscaled CoO than in the bulk. Similar excess broadening has previously been observed for the precessional mode in both ferromagnetic and antiferromagnetic nanoparticles[77] and thin films[24,78]. It is explained by acknowledging that the lifetime of the q=0 spin wave is limited by its decay via scattering into spin wave modes with q≠0, and not by the spin-lattice relaxation time, which is known to be much longer[79–81]. In thin films, the q=0 mode decays into a pair of magnons with ±q via scattering from random fields at the film surface[82–84]. Fig. 8 indicates that Γ_1(q) is the same for CoO shells that are 1.7 nm thick and 4.5 nm thick, which consequently have very different surface areas. For this reason, we consider it more likely that impurity scattering and not surface scattering is the primary decay mechanism for the magnetic excitations with nonzero wave vector in Co/CoO core-shell nanoparticles in thermal equilibrium[79,85,86], a result that has been separately proposed for ultrathin antiferromagnetic films[87].

The most striking differences between the inelastic scattering in the bulk and nanoscaled systems are its relative intensities I(q). Fig. 6b shows that the 3 meV inelastic peak is only observed for a limited range of wave vectors near the antiferromagnetic q_{AF} in powdered bulk CoO, while it is much more diffuse in nanoscaled CoO, where we find $I(q) \approx I_0 + Aq^2$ (Fig. 3d). It is possible that at least some of the q-dependent part of this intensity arises from enhanced coupling of the E_1 excitation to a dispersing relaxational mode, perhaps having the same source as the large and q-dependent broadening of the inelastic linewidth. However, this explanation cannot reasonably explain the massive enhancement of the intensity of the E_1 excitation in the nanoparticles. Fig. 3d shows that the intensity of the 3 meV E_1 peak, when normalized to the known amounts of CoO present in each sample, is almost 500 times stronger in nanoscaled CoO than in bulk, and for the 20 meV spin wave, a factor of 40 larger in nanoscaled CoO than in the bulk (Fig. 7b). Considering the sum rule that limits the total magnetic scattering possible per gram CoO, this effect cannot be an overall amplification of the scattering in nanoscaled CoO, but rather a dramatic shift of spectral weight into the finite window of wave vectors and energies accessed in our experiments. A comparison of Fig. 1c and Fig. 4a shows that the spin wave population is strongly shifted towards larger wave vectors and smaller wavelengths in nanoscaled CoO, relative to bulk CoO. It is most likely that this excess scattering comes at the expense of scattering that would be elastic in bulk CoO, such as the magnetic Bragg peaks. Similarly, the spectral weight that corresponds to long wave length quasielastic and inelastic scattering, now prohibited by the requirement that excitations must have $q \geq \pi/d$, pushes this spectral weight to higher energies and shorter time scales. Accordingly, Fig. 7 shows that this effect is an order of magnitude stronger at low energies ($E \leq 10$ meV) than at large ($20 \leq E \leq 30$ meV). This dynamical broadening and shifting of spin wave intensity to larger wave vectors was predicted in numerical studies of very small ferromagnetic particles[12], and it is interesting and perhaps surprising that this effect is apparently still robust in our CoO shells, which have as many as 10^4 - 10^5 Co moments.

In conclusion, we report here the observation via inelastic neutron scattering measurements of new low energy excitations in Co core/CoO shell nanoparticles, which were also shown to be present in powdered bulk CoO. While previous measurements have focussed on q=0 precessional modes or surface modes, this is the first observation of a magnetic excitation with length and time scales that are well matched to those involved in the reversal of nanoparticle magnetization. The energies and dispersions of these excitations are very similar in bulk and nanoscaled CoO, and our analysis suggests that the exchange splitting of the crystal field and spin -orbit split Co^{2+} states is much weaker than previously considered. Dramatic finite size effects were observed in the nanoparticles. The excitation linewidths are much broader in the CoO nanoparticle shells than in powdered bulk CoO, reflecting a greater role for impurity scattering in limiting the excitation lifetime in the former. While the magnetic excitation is found only near the magnetic ordering wave vector in powdered bulk CoO, this mode is diffuse in the nanoparticle shells. We present evidence that there is a massive rearrangement of magnetic spectral weight to larger energies in nanoscaled CoO, relative to the bulk. Our experiments indicate that the magnetic excitations that modulate the nanoparticle magnetization are on average shorter ranged and shorter lived than their analogs in bulk CoO.

V. ACKNOWLEDGMENTS

We are grateful to S. Shapiro for useful discussions, and to Jack Simonson for assistance with magnetization measurements. Work at BNL was carried out under the auspices of the U.S. Department of Energy, Office of Basic Energy Sciences under Contract No. DE-AC02-98CH1886 (MF and MCA), and at the Brookhaven Center for Functional Nanomaterials under Contract No. DE-AC02-98CH10886. Work at NIST is supported in part by the NSF under Agreement No. DMR-0454672. Work at the Spallation Neutron Source was sponsored by the Scientific User Facilities Division, Department of Energy, Office of Basic Energy Sciences. X.T. and W. D. are partially supported by the University of New Hampshire.

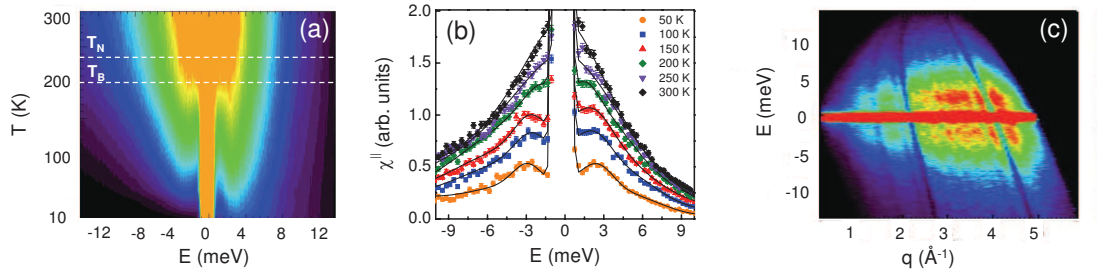

FIG. 1: (a) (Color online) The q-integrated scattered intensity I(E) at different temperatures for Co/CoO nanoparticles (sample Co/CoO#4). Dashed lines indicate the onset of antiferromagnetic order at T_N, and the dynamical blocking of the Co cores at the blocking temperature T_B. (b) Energy dependence of χ''(E) for a constant wave vector cut 0.12 $\AA^{-1}$ wide and centered at q = 1.27 $\AA^{-1}$ for Co/CoO nanoparticle sample #4 at different temperatures, as indicated. Solid lines are the fits, described in the text. (c) The scattered intensity I(q,E) at 150 K for Co/CoO nanoparticles (sample Co/CoO#4). Dark curved lines are shadows from the radial collimator.

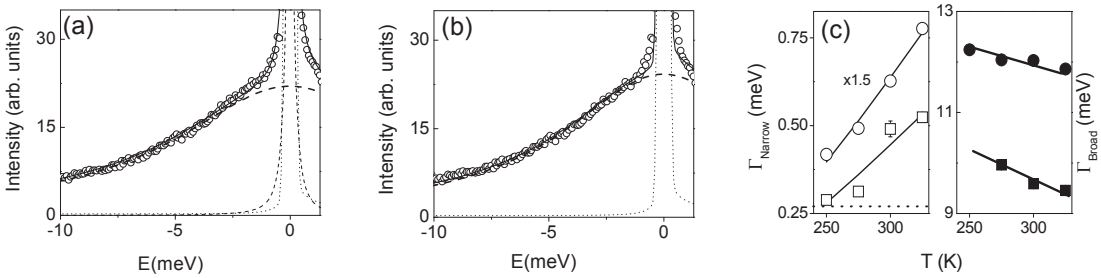

FIG. 2: (a) Scattered intensity I(q,E) for sample Co/CoO #4 at 300 K for a constant wave vector cut 0.3 $\AA^{-1}$ wide, centered at q=2.45 $\AA^{-1}$. Solid line is the fit, consisting of a broad Lorentzian I_{Broad} (bold dashed line) and a narrow Lorentzian I_{Narrow} (dashed line), and a resolution broadened delta function (dotted line), representing the elastic scattering. (b) An alternate presentation of the same data as (a), but with the narrow Lorentzian component omitted from the fit. Note the excess scattered intensity at low energies that is not captured by the new fit, indicated by the solid line, consisting here of a broad Lorentzian I_{Broad} (bold dashed line) and a resolution broadened delta function (dotted line), representing the elastic scattering. (c) Left panel: the temperature dependencies of the core reversal linewidths Γ_{Narrow} (□=Co/CoO#3, ○=Co/CoO#4). Solid lines are fits to an Arrhenius expression, horizontal dotted line is DCS resolution. Right panel: temperature dependencies of the linewidths Γ_{Broad} (■=Co/CoO#3, ●=Co/CoO#4). Solid lines are guides for the eye.

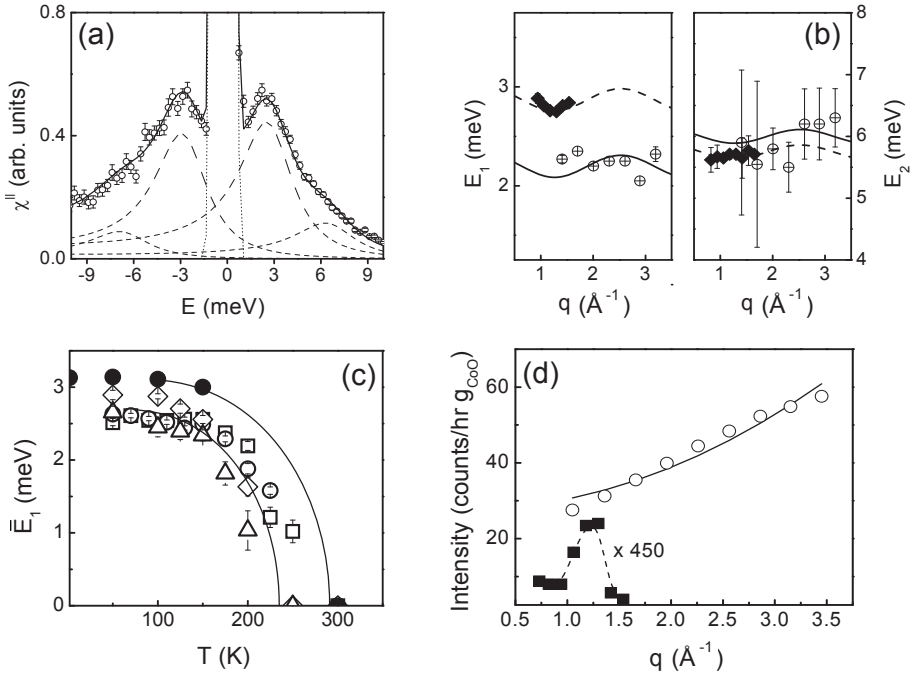

FIG. 3: (a) Energy dependence of $\chi^{''}$(E) for sample Co/CoO #4 at 50 K for a constant wave vector cut with a width of 0.12 $\AA^{-1}$ centered at q=1.27$\AA^{-1}$. Solid line is the fit, consisting of two pairs of inelastic Lorentzians, the first centered at $E_1 \approx \pm 3$ meV (long dashed line)and the second at $E_2 \approx \pm$ 6 meV (short dashed line), and a resolution broadened delta function (dotted line), representing the elastic scattering. (b) The wave vector dependence of the inelastic excitation energies E_1(left panel) and E_2(right panel) at 150 K, measured for Co/CoO#4 ($\oplus$) and powdered bulk CoO ($\blacklozenge$). Solid lines are the best fits to nanoparticle E_1(q) and E_2(q), described in the text, dashed lines are for powdered bulk CoO. (c) Temperature dependencies of the wave vector averaged value of $\bar{E_1}$ in our different samples ($\square$=Co/CoO#1, $\circ$=Co/CoO#2, $\diamond$=Co/CoO#3, $\triangle$=Co/CoO#4,$\triangledown$=Co/CoO#5, and $\bullet$= powdered bulk CoO). Solid lines are mean field fits with T_N=235 K (nanoparticle samples) and T_N=293 K (bulk CoO powder). (d) The q-dependence of the intensity of the inelastic peak at $E_1 \approx$3 meV at 150 K for Co/CoO#4 nanoparticles ($\bigcirc$) and powdered bulk CoO ($\blacksquare$, multiplied by 450 for comparison). The solid line is the fit of Co/CoO#4 with the following function $I(q)=I_0+Aq^2$. The dashed line is guide for the eye.

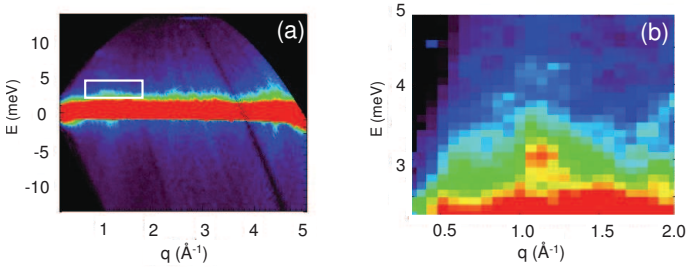

FIG. 4: (a) The scattered intensity I(q,E) at 50 K for powdered bulk CoO. (b) An expanded view of the outlined area in (a), demonstrating enhanced scattering near the antiferromagnetic wave vector q_{AF}=1.27 $\AA^{-1}$ of bulk CoO.

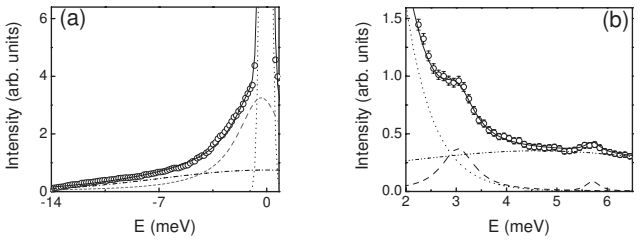

FIG. 5: (a) The scattered intensity I(q,E) at 300 K for a constant wave vector cut with a width of 0.12 $\AA^{-1}$ centered at q_{AF}=1.27$\AA^{-1}$ for powdered bulk CoO. Solid line shows the fit, described in the text and consisting of a quasielastic Lorentzian (dashed line), a broad background (dotted-dashed line) and a resolution broadened delta function (dotted line), representing the elastic scattering. (b) The scattered intensity I(q,E) at 50 K for a constant wave vector cut with a width of 0.12 $\AA^{-1}$ centered at q_{AF}=1.27$\AA^{-1}$ for powdered bulk CoO. Solid line shows the fit, described in the text, consisting of two inelastic Lorentzians(dashed lines) centered near E_1 ≈3 meV and E_2 ≈5.7 meV, as well as a broad background function (dotted-dashed line) and a resolution broadened delta function (dotted line) representing the elastic scattering.

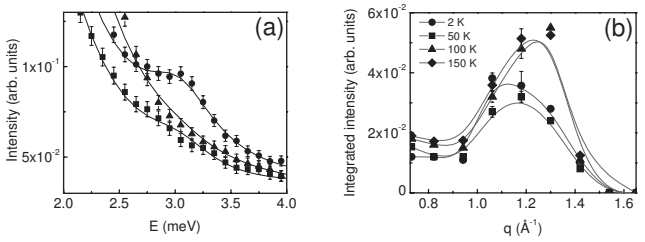

FIG. 6: (a) The scattered intensity I(q,E) for powdered bulk CoO at 50 K, for constant wave vector cuts with widths of 0.12 $\AA^{-1}$ centered at 0.73$\AA^{-1}$ (■), q_{AF}=1.27$\AA^{-1}$(●), and 1.65 $\AA^{-1}$ (▲). Solid lines are fits described in text. (b) The wave vector dependencies of the integrated intensity of the fitted E_1 ≈3 meV inelastic peaks of powdered bulk CoO, measured at different temperatures, as indicated. Solid lines are guides for the eye.

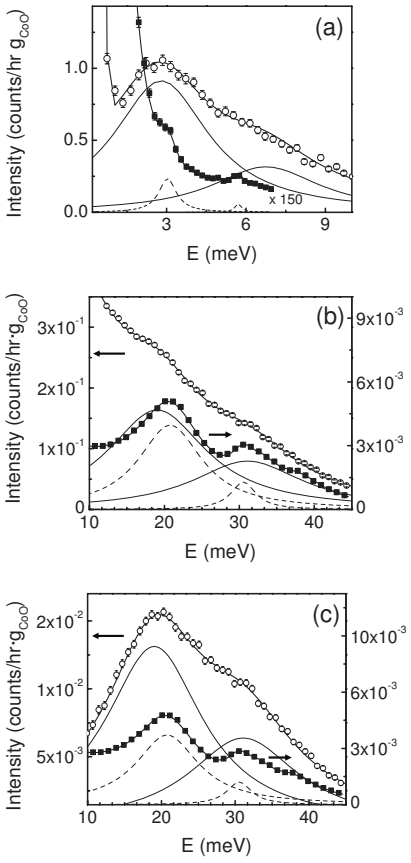

FIG. 7: (a) The scattered intensities I(q,E), normalized to the CoO mass, for powdered bulk CoO (■, multiplied by 150 for ease of comparison) and Co/CoO#4 (◯) at 50 K, for constant wave vector cuts with widths of 0.12 $\AA^{-1}$, centered at q_{AF}=1.27$\AA^{-1}$. Solid lines are fits described in text. The Lorentzian functions associated with the inelastic excitations at E_1 ≈3 meV and E_2 ≈6 meV are shown for Co/CoO#4 as solid lines, and for powdered bulk CoO as dashed lines. (b) Same as (a), but for 150 K, and with larger energy transfers (λ=1.22 $\AA$). Here the fitted inelastic peaks for Co/CoO#4 (left axis) are given as solid lines, and dashed lines for powdered bulk CoO (right axis). (c) Same as (b) but with background scattering removed.

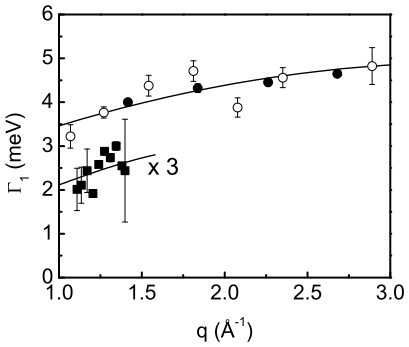

FIG. 8: The wave vector dependencies of the E_1 ≈3 meV inelastic peak in Co/CoO#4 (◯, 4.5 nm CoO thickness), Co/CoO#1 (•, 1.7 nm CoO thickness), and powdered bulk CoO (■), multiplied by three for comparison. Solid lines are guides for the eye.

[1] J. Nogués and I. Schuller, J. Magn. and Magn. Mater. **192**, 203 (1999).
[2] R. L. Stamps, J. Phys. D: Appl. Phys. **33**, R247 (2000).
[3] J. Nogués, J. Sort, V. Langlais, V. Skumryev, S. Suriñach, J. S. Muñoz, and M. D. Baró, Physics Reports **422**, 65 (2005).
[4] V. L. Safonov and H. N. Bertram, J. Appl. Phys. **87**, 5508 (2000).
[5] P. B. Visscher, D. M. Apalkov, and F. Feng, IEEE Transactions on Magnetics **38**, 2523 (2002).
[6] T. J. Silva, P. Kabos, and M. R. Pufall, Appl. Phys. Letts. **81**, 2205 (2002)
[7] V. L. Safonov, J. Appl. Phys. **95**, 7145 (2004).
[8] K. L. Livesey, M. P. Kostylev, and R. L. Stamps, Phys. Rev. B **75**, 174427 (2007).
[9] F. Wegelin, D. Valdaitsev, A. Krasyuk, S. A. Nepijko, G. Schönhense, H. J. Elmers, I. Krug, and C. M. Schneider, Phys. Rev. B **76**, 134410 (2007).
[10] D. A. Garanin and H. Kachkachi, Phys. Rev. B **80**, 014420 (2009).
[11] R. L. Stamps, Adv. Funct. Mats. **20**, 2380 (2010).
[12] P. V. Hendriksen, S. Linderoth, and P. -A. Lindgård, Phys. Rev. B **48**, 7259 (1993).
[13] J. M. Wesselinowa, and I. Apostolova, J. Phys.: Condensed Matter, **19**, 216208 (2007).
[14] S. Mørup and B. R. Hansen, Phys. Rev. B **72**, 024418 (2005).
[15] M. F. Hansen, F. Bødker, S. Mørup, K. Lefmann, K. N. Clausen, and P. A. Lindgård, Phys. Rev. Lett. **79**, 4910 (1997).
[16] M. F. Hansen, F. Bødker, S. Mørup, K. Lefmann, K. N. Clausen, P. A. Lindgård, J. Magn. and Magn. Mater. **221**, 10 (2000).
[17] S. N. Klausen, K. Lefmann, P. -A. Lindgård, K. N. Clausen, M. F. Hansen, F. Bødker, S. Mørup, and M. Telling, J. Magn. and Magn. Mater. **266**, 68 (2003).
[18] M. Hennion, C. Bellouard, I. Mirebeau, J. L. Dormann, and M. Nogues, Europhys. Lett. **25**, 43 (1994).
[19] K. Lefmann, F. Bødker, S. N. Klausen, M. F. Hansen, K. N. Clausen, P.-A. Lindgård, and S. Mørup, Europhys. Lett. **54**, 526 (2001).
[20] S. N. Klausen, K. Lefmann, P.-A. Lindgård, L. Theil Kuhn, C. R. H. Bahl, C. Frandsen, S. Mørup, B. Roessli, N. Cavadini, and C. Niedermayer, Phys. Rev. B **70**, 214411 (2004).
[21] S. Mørup, D. E. Madsen, C. Frandsen, C. R. H. Bahl, and M. F. Hansen, J. Phys.: Condensed Matter **19**, 213202 (2007).
[22] R. L. Stamps, R. E. Camley, and R. J. Hicken, Phys. Rev. B **54**, 4159 (1996).
[23] A. Ercole, W. S. Lew, G. Lauhoff, E. T. M. Kernohan, J. Lee, and J. A. C. Bland, Phys. Rev. B **62**, 6429 (2000).
[24] A. Ercole, W. S. Lew, G. Lauhoff, E. T. M. Kernohan, J. Lee, and J. A. C. Bland, Phys. Rev. B **62**, 6429 (2000).
[25] S. M. Rezende, A. Azevedo, M. A. Lucena, and F. M. de Aguiar, Phys. Rev. B **63**, 214418 (2001).
[26] M. C. Weber, H. Nembach, H. Hillebrands, and J. Fassbender, J. Appl. Phys. **97**, 10A701 (2005).
[27] V. P. Shilov, Yu. L. Raikher, J.-C. Bacri, F. Gazeau, and R. Perzynski, Phys. Rev. B **60**, 11902 (1999).
[28] V. P. Shilov, J.-C. Bacri, F. Gazeau, F. Gendron, R. Perzynski, and Yu. L. Raikher, J. Appl. Phys. **85**, 6642 (1999).
[29] V. J. Minkiewicz, M. F. Collins, R. Nathans, and G. Shirane, Phys. Rev. **182**, 624 (1969).
[30] C. J. Glinka, V. J. Minkiewicz, and L. Passell, Phys. Rev. B **16**, 4084 (1977).
[31] J. Sakurai, W. J. L. Buyers, R. A. Cowley, and G. Dolling, Phys. Rev. **167**, 510 (1968).
[32] K. Tomiyasu and S. Itoh, J. Phys. Soc. Japan **75**, 084708 (2006).
[33] Z. Yamani, W. J. L. Buyers, R. A. Cowley, and D. Prabhakaran, Physica B **403**, 1406 (2008).
[34] Z. Yamani, W. J. L. Buyers, R. A. Cowley, and D. Prabhakaran, Can. J. Phys. **88**, 1 (2010).
[35] M. R. Daniel and A. P. Cracknell, Phys. Rev. **177**, 932 (1969).
[36] I. G. Austin and E. S. Garbett, J. Phys. C: Solid State Physics **3**, 1605 (1970).
[37] Ch. Kant, T. Rudolf, F. Schrettle, F. Mayr, J. Deisenhofer, P. Lunkenheimer, M. V. Eremin, and A. Loidl, Phys. Rev. B **78**, 245103 (2008).
[38] J. Kanamori, Prog. Theor. Phys. (Kyoto) **17**, 177 (1956).
[39] T. Yamada and O. Nakanishi, J. Phys. Soc. Japan **36**, 1304 (1974).
[40] A. Boussendel, N. Baadji, A. Haroun, H. Dreyssé, and M. Alouani, Phys. Rev. B **81**, 184432 (2010).
[41] X. Qiu, T. Proffen, J. F. Mitchell, and S. J. L. Billinge, Phys. Rev. Lett. **94**, 177203 (2005).
[42] A. S. Masadeh, E. S. Bozin, C. L. Farrow, G. Paglia, P. Juhas, S. J. L. Billinge, A. Karkamkar, and M. G. Kanatzidis, Phys. Rev. B **76**, 115413 (2007).
[43] C. L. Farrow and S. J. L. Billinge, Acta. Cryst. **A65**, 232 (2009).
[44] A. Guinier, *X-Ray Diffraction in Crystals, Imperfect Crystals, and Amorphous Bodies,*(Freeman San Francisco 1963).
[45] K. Kodama, S. Iikubo, T. Taguchi, and S. Shamoto, Acta Cryst. A **62**, 444 (2006).
[46] B. Gilbert, J. Appl. Cryst. **41**, 554 (2008).
[47] S. E. Inderhees, J. A. Borchers, K. S. Green, M. S. Kim, K. Sun, G. L. Strycker, and M. C. Aronson, Phys. Rev. Lett. **101**, 117202 (2008).
[48] B. Palosz, E. Grzanka, S. Gierlotka, S. Stel'Makh, R. Pielaszek, U. Bismayer, J. Neuefeind, H. P. Weber, and W. Palosz, Acta Phys. Pol. A **102**, 57 (2002).
[49] T. Egami and S. J. L. Billinge, *Underneath the Bragg Peaks: Structural Analysis of Complex Materials* , (Pergamon, Ansterdam 2003).
[50] A. Cehovin, C. M. Canali, and A. H. MacDonald, Phys. Rev. B **68**, 014423 (2003).
[51] S. Mørup, C. Frandsen, F. Bødker, S. N. Klausen, K. Lefmann, P.-A. Lindgård, and M. F. Hansen, Hyperfine Interactions **144 − 145**, 347 (2002).
[52] S. Carretta, P. Santini, G. Amoretti, T. Guidi, J. R. D. Copley, Y. Qiu, R. Caciuffo, G. Timco, and R. E. P. Winpenny, Phys. Rev. Lett. **98**, 167401 (2007).
[53] P. Santini, S. Carretta, G. Amoretti, T. Guidi, R. Caciuffo, A. Caneschi, D. Rovai, Y. Qiu, and J. R. D. Copley, Phys. Rev. B **71**, 184405 (2005).
[54] V. F. Puntes, K. M. Krishnan, and A. P. Alivisatos, Science **291**, 2115 (2001).
[55] M. Feygenson, Y. Yiu, A. Kou, K. S. Kim, and M. C.

Aronson, Phys. Rev. B **81**, 195445 (2010).
[56] J. P. Chen, C. M. Sorensen, K. J. Klabunde, and G. C. Hadjipanayis, Phys. Rev. B **51**, 11527 (1995).
[57] http://www.ncnr.nist.gov/dave
[58] C. Mathieu, J. Jorzick, A. Frank, S. O. Demokritov, A. N. Slavin, B. Hillebrands, B. Bartenlian, C. Chappert, D. Decanini, F. Rousseaux, and E. Cambril, Phys. Rev. Lett. **81**, 3968 (1998).
[59] K. Lefmann, F. Bødker, M. F. Hansen, H. Vazquez, N. B. Christensen, P.-A. Lindgård, K. N. Clausen, and S. Mørup, Eur. Phys. J. D **9**, 491 (1999).
[60] H. Schultheiss, S. Schäfer, P. Candeloro, B. Leven, B. Hillebrands, and A. N. Slavin, Phys. Rev. Lett. **100**, 047204 (2008).
[61] E. P. Wohlfarth, *Ferromagnetic Materials* ed. E. P. Wohlfarth, (North-Holland, Amsterdam 1980).
[62] K. N. Clausen, F. Bødker, M. F. Hansen, L. Theil Kuhn, K. Lefmann, P.-A. Lindgård, S. Mørup, and M. Telling, Physica B **276**, 830 (2000).
[63] C. G. Shull, W. A. Strauser, and E. O. Wollan, Phys. Rev. **83**, 333 (1951).
[64] W. L. Roth, Phys. Rev. **110**, 1333 (1958).
[65] B. van Laar, J. Schweizer, and R. Lemaire, Phys. Rev. **138A**, 584(1965).
[66] W. Jauch, M. Reehuis, H. J. Bleif, F. Kubanek, and P. Pattison, Phys. Rev. B **64**, 052102 (2001).
[67] T. Nagamiya and K. Motizuki, Rev. Mod. Phys. **30**, 89 (1958).
[68] M. Tachiki, J. Phys. Soc. Japan **19**, 454 (1964).
[69] R. Alben, J. Appl. Phys. **40**, 1112 (1969).
[70] S. Shi and V. Staemmler, Phys. Rev. B **52**, 12345 (1995).
[71] R. C. Milward, Phys. Lett. **16**, 244 (1965).
[72] R. R. Hayes and C. H. Perry, Solid State Commun. **13**, 1915 (1973).
[73] H-h. Chou and H. Y. Fan, Phys. Rev. B **13**, 3924 (1976).
[74] V. Wagner and W. Drexel, J. Magn. Magn. Mater. **2**, 106 (1976).
[75] M. El-Batanouny, J. Phys.: Condensed Matter **14**, 6281 (2002).
[76] B. I. Halperin and P. C. Hohenberg, Phys. Rev. Lett. **19**, 700 (1967).
[77] TheilKuhn L, K. Lefmann, C. R. H. Bahl, S. N. Ancona, P. A. Lindgård, C. Frandsen, D. E. Madsen and S. Mørup, Phys. Rev. B **74**, 184406 (2006).
[78] R. L. Stamps, R. E. Camley, and R. J. Hicken, J. Appl. Phys. **81**, 4485 (1997).
[79] C. Kittel and E. Abrahams, Rev. Mod. Phys. **25**, 233 (1953).
[80] A. Vaterlaus, T. Beutler, and F. Meier, Phys. Rev. Lett. **67**, 3314 (1991).
[81] E. Beaurepaire, J. C.- Merle, A. Daunois, and J. Y-. Bigot, Phys. Rev. Lett. **76**, 4250 (1996).
[82] C. Mathieu, M. Bauer, B. Hillebrands, J. Fassbendder, G. Güntherodt, R. Jungblut, J. Kohlhepp, and A. Reinders, J. Appl. Phys. **83**, 2863 (1998).
[83] R. Arias and D. L. Mills, Phys. Rev. B **60**, 7395 (1999).
[84] S. M. Rezende, A. Azevedo, M. A. Lucena, and F. M. de Aguiar, Phys. Rev. B **63**, 214418 (2001).
[85] A. M. Clogston, H. Suhl, L. R. Walker, and P. W. Anderson, J. Phys. Chem. Solids **1**, 129 (1956).
[86] A. M. Clogston, H. Suhl, L. R. Walker, and P. W. Anderson, Phys. Rev. **101**, 903 (1956).
[87] J. M. Pereira and M. G. Cottam, Phys. Rev. B **68**, 104429 (2003).